The Effect of Silica Nanoparticles on the Thermomechanical Properties of Polystyrene

E. Kontou, G. Anthoulis

Department of Applied Mathematical and Physical Sciences, Section of Mechanics, National Technical University of Athens, 5 Heroes of Polytechnion, GR-15773 Athens, Greece

ABSTRACT: A series of polystyrene (PS)/SiO$_2$ nanocomposites were prepared. Silica nanoparticles with an average diameter of 16 nm were used, and treated with dimethyldichlorosilane, while their weight fraction varied from 4 up to 10%. The viscoelastic-thermomechanical properties of the nanocomposites and their interrelation with the material's structure were studied with various experimental techniques. Scanning electron microscopy, differential scanning calorimetry, dynamic mechanical analysis, and tensile testing at three different temperatures were applied. The stress–strain curves at 85°C, where the material's viscoplastic response is manifested, were simulated through a plasticity model, developed in previous works. The 4% weight fraction was found to be the optimum one for the enhancement of the thermomechanical properties. © 2007 Wiley Periodicals, Inc. J Appl Polym Sci 105: 1723–1731, 2007

Key words: polystyrene; nanocomposites; silica; viscoplasticity

INTRODUCTION

Polymer nanocomposites are a novel class of composite materials that exhibit a dramatic improvement in stiffness, strength, and thermal properties compared to polymers, or conventional composite materials. These superior properties result from the fact that nanocomposites have much larger surface area per unit volume, since one of the constituents has dimensions that range between 1 and 100 nm. Since most of chemical and physical interactions are influenced by surfaces, the properties of a nanostructured material can be substantially different from those of a conventional composite material, with the same composition.[1,2]

Parameters such as filler aspect ratio, filler mechanical properties, the quality of adhesion may strongly affect the degree of reinforcement.[3] A lot of works have been dealt with various types of nanosized fillers and various methods of polymer/nanocomposite technology.[1,4,5] Moreover, a variety of polymer matrices such as epoxies,[6,7] elastomers,[8,9] polyolefines,[10,11] have been studied in combination with nanosized fillers, leading to various degrees of reinforcement.

Multiple techniques can be used to analyze nanocomposites and quantify the filler dispersion and the material morphology. The interrelation between rheological properties and nanocomposite morphology has been extensively studied.[12–16]

Along with the improved chemical and physical properties of nanocomposites the mechanical properties such as stiffness, strength, and toughness have been studied because of their great potential in engineering. In spite of the fact that there is a large number of works dealing with material's synthesis and characterization of polymer nanocomposites, the fundamental mechanisms for mechanical property improvement are not yet completely defined.[17–20] There is a large number of works dealing with mechanics based models, which describe successfully the mechanical properties of conventional polymer composites and, recently, some efforts have been made to apply these models on the thermal and mechanical properties of polymer nanocomposites.[21–23]

In the present work, nanocomposites based on polystyrene (PS) reinforced by silica nanoparticles at various weight fractions, and prepared with a simple melt mixing procedure, were studied. The aim of the present study was to find the optimum silica content for the PS matrix applying a conventional melt mixing technique for the preparation of PS nanocomposites. The degree of reinforcement, as well as the overall viscoelastic response was studied in terms of dynamic mechanical analysis (DMA) tests, differential scanning calorimetry (DSC) experiments, as well as mechanical testing in terms of tension at three different temperatures. Tensile stress–strain data at a

high temperature, below T_g, where material visco-plasticity is manifested, were simulated with a model developed and used in previous work.[24] The results of the various experimental techniques applied, were combined with model simulations, providing useful evidence about the PS-nanocomposites morphology and quality of dispersion. The above analysis lead to the result that 4% per weight is the optimum silica content, characterized by the better particle distribution and improved mechanical properties.

MATERIALS

PS under the commercial name Styron 637, provided by Dow Chemicals, with a density of 1.05 g/cm^3 (ISO 1183) and a melt mass flow index of 2.5 (g/10 min) was used as a matrix. Silica Aerosil R972 (supplied by Degussa Chemicals) was used for the preparation of the nanocomposites under investigation. Aerosil R972 is a hydrophobic fumed silica after treated with dimethyldichlorosilane based on a hydrophilic fumed silica, with a specific surface area of 130 m^2/g. The average primary particle size is 16 nm.

Three percentage contents of silica were studied namely 4, 8, and 10% per weight. The pure matrix was also studied. Mixing of Aerosil silica with the PS matrix was performed with a Brabender mixer. The optimum processing conditions were selected to be as follows: the mixing temperature was 170°C and the screw rotation speed was 40 rpm. The silica powder was fed to the polymer melt carefully to achieve the optimum particle dispersion. Afterwards, the materials were compression molded at 130°C, using a thermopress and a special mold of 2 mm thickness. The selection of the processing conditions is based on the results of a previous study.[10] All material types were thermally treated at 90°C (which is close to the T_g of the materials) for 2 h to erase any kind of prehistory.

EXPERIMENTAL METHODS

Scanning electron microscopy (SEM) images of fracture surfaces were obtained using a Leitz AMR 1600T scanning microscope, operated at an accelerated voltage of 20 kV. All the studied samples were coated with carbon black to avoid charging under the electron beam.

Calorimetric measurements were carried out using a Setaram DSC 141 instrument, calibrated with an Indium standard. All materials were heated with a constant heating rate of 5°C/min from 23°C up to 150°C and the corresponding thermogram was recorded.

Specific heat values C_p were also measured, using an appropriate software, connected to the aforemen-

tioned device. The sudden change ΔC_p of C_p, appearing at the zone of glass-transition temperature, could then be evaluated.

DMA experiments were performed using the Perkin–Elmer DMA 7e instrument. The mode of deformation applied was the three-point bending system, and the mean dimensions of sample plaques were 2 mm × 4mm × 20 mm. The temperature range varied from ambient temperature up to 110°C. The temperature dependent behavior was studied by monitoring changes in force and phase angle, keeping the amplitude of oscillation constant. Three different frequencies, namely 0.1, 1, and 10 Hz, were examined and the heating rate was 5°C/min. The storage and loss moduli as well as loss tangent curves versus temperature were evaluated.

Tensile measurements were carried out with an Instron 1121 type tester, at 20°C, as well as at 85 and 100°C. The dumbbell type specimens, according to ASTM D 638, were of a gauge length of 30 mm, and the applied crosshead speed in all cases was 0.5 mm/min. This value corresponds to an effective strain rate of 2.77×10^{-4} s^{-1}. Experiments at high temperatures were executed with a high temperature chamber series 3119-406 of Instron Ltd.

For tests performed at 20°C, the deformation could be measured very accurately with an experimental procedure, which is based on a noncontact method with a laserextensometer, described in detail in a previous work.[25]

RESULTS AND DISCUSSION

SEM results

Figures 1–3 show the SEM micrographs of PS-4% SiO$_2$, 8% SiO$_2$, and 10% SiO$_2$, respectively. From
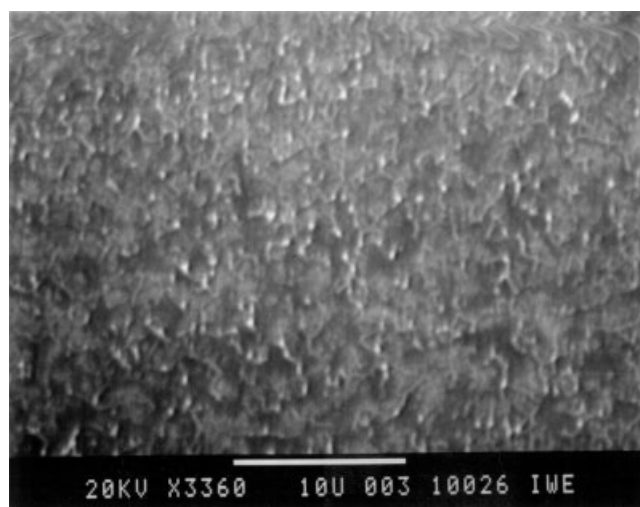
F1-F3

Figure 1 SEM micrographs of the PS-4% SiO$_2$. Scale bar corresponds to 10 μm.
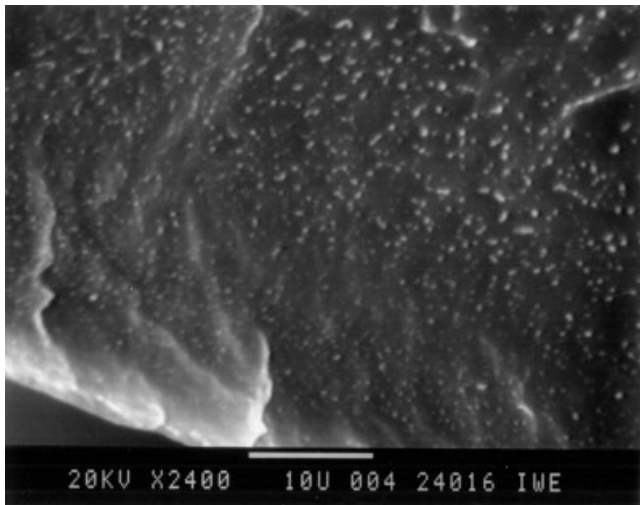
Figure 2 SEM micrographs of the PS-8% SiO_2. Scale bar corresponds to 10 μm.

these figures, where the scale bar corresponds to 10 μm, it is observed that all sample types contain agglomerates with varying size of the dispersed phase. In the PS-4% SiO_2 material type the average particle size is of the order of 300 nm, while there are observed particles of the order of 100 nm, as well as a few agglomerates of greater size. For a silica content of 8% per weight the material exhibits agglomerates with an average particle size of 500 nm. At a silica content of 10% the number of agglomerates increased, and they were in average of the order of 1.5 μm. These results are in good agreement with the ones reported by Wu et al.,[26] who reported that increasing the silica content in polypropylene nanocomposites leads to larger agglomerates.

These observations are also in accordance with the fact that the available nanoparticles are generally in
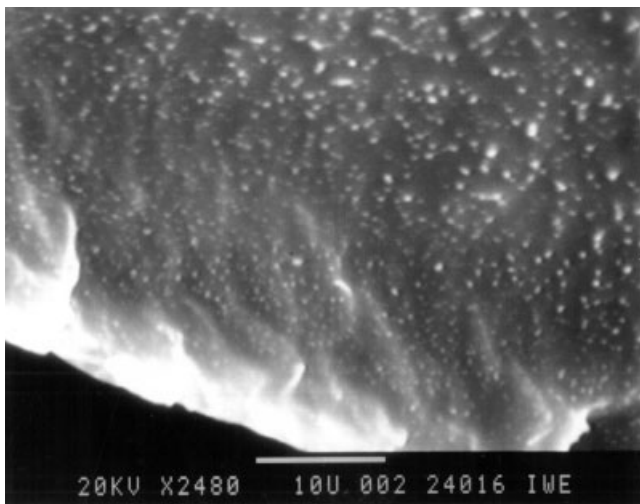
the form of agglomerates and it is rather hard to be dispersed in their initial dimensions. This is due to the strong interaction among them, the procedure of melt mixing that was followed and the high melt flow index (which is a property related with the melt viscosity) of the polymeric matrix.

DMA results

DMA results may provide useful information about the structure and viscoelastic properties of the materials, especially when these results are extended in a wide frequency range. For this purpose, master curves for storage and loss modulus E' and E'' respectively, for all material types examined, were calculated and plotted, applying the time–temperature superposition principle. This principle is only valid when the relaxation times have the same temperature dependence and this is not the case for most of the materials, which are rather characterized by thermorheological complexity. Master curves, in respect to a reference temperature of 95°C are plotted in Figures 4–7 for pure PS, PS-4%, PS-8%, and PS-10% respectively. As it is observed from these figures, in all sample types a satisfactory master curve is obtained with a very low data fluctuation, which is encouraging evidence for the application of time–temperature superposition principle. The transition region of E' exhibits a very slight shifting to higher frequencies as silica content increases. The same effect is observed from the E'' curves, where the frequency with the maximum value of loss modulus shifts from 0.38 Hz for pure PS to 3.10 Hz for PS-10%. In pure PS (Fig. 4) the plateau region at high frequencies is followed by a transition region, which is dissipative, i.e., strongly viscoelastic. At low frequencies, a terminal region characterized by a slight levelling-off is observed. In those regions E'' remains higher than E', and there is one frequency where E'
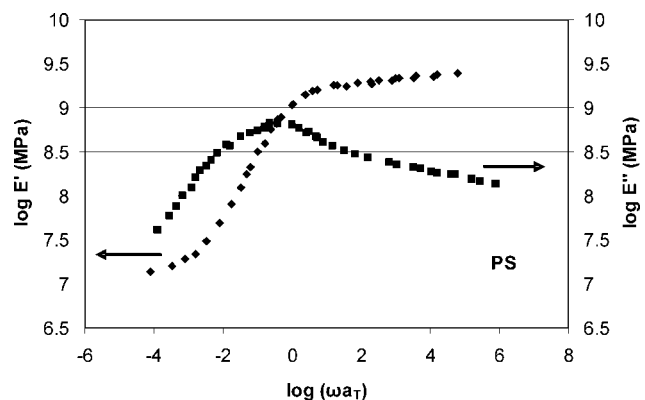

Figure 4 Master curves of storage modulus E' and loss modulus E'' of pure PS in a reduced frequency scale, at a reference temperature of 95°C.
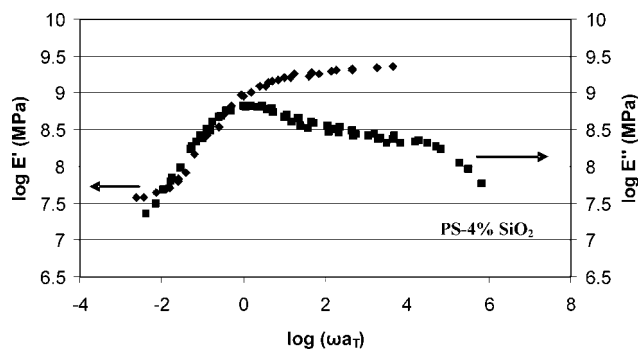

Figure 3 SEM micrographs of the PS-10% SiO_2. Scale bar corresponds to 10 μm.

Figure 5 Master curves of storage modulus E' and loss modulus E'' of PS-4% SiO_2 in a reduced frequency scale, at a reference temperature of 95°C.

and E'' crossover. The particle distribution inside the polymer matrix is a key factor,[5] that determines the rheological response of nanocomposites. For PS-4%, PS-8%, and PS-10% samples (Figs. 5–7), the high frequency plateau is slightly increased, indicating the filler reinforcing effect, but more substantial changes are observed at lower frequencies. In Figure 5, two crossover frequencies namely 0.63 and 0.01 Hz for PS-4% appear, revealing three frequency regions: the high frequency region related with the glassy plateau, the intermediate region where E'' values are close to those of E', and the low frequency range where a secondary plateau is obtained. The existence of this levelling-off is related with the polymer chains and silica nanoparticles interrelation, probably due to the network structuring from the estimated better dispersed particles, in comparison with the other material types. In the work by Zhao et al.[5] an analogous relation between G' and G'' is attributed to the increment of dispersion level and, therefore, a more solidlike behavior should be exhibited. Additionally, the existence of two crossover frequencies denotes a better particle dispersion[5] and this effect has been observed only for PS-4% material type.

At higher silica content, PS-8% presented in Figure 6, it is observed that E' is always higher than E'', indicating that, due to the increased presence of fil-
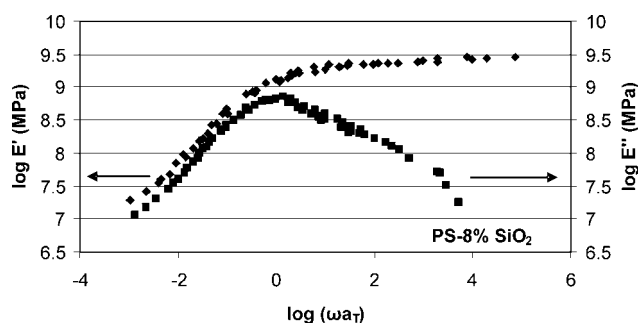
ler, the solid like behavior is more dominant. However, the low frequency plateau is very slight when compared to that of PS-4% (Fig. 5). This effect can be attributed to the existence of more and larger agglomerates at this filler content, which cannot act as a physical network and consequently mechanically effective. This remark is reinforced by the SEM results, where it was found that larger agglomerates exist in the case of PS-8%. The PS-10%, presented in Figure 7, was found to exhibit a reversed behavior, namely it exhibits a relation between E' and E'' similar to that of pure PS. There is one crossover frequency at about 1.39 Hz, and at low frequencies E'' is higher that E'.

To further support the aforementioned conclusions we are referring to a recent work by Bartholome et al.[27] In their study, PS/nanocomposites do not show any terminal flow zone, as the pure matrix does. Instead they exhibit a secondary plateau, which is related to the density and strength of a network structure, formed by van Der Waals or H-bonding interactions between the filler particles. In the same work, it is reported that when PS chains are grafted onto silica, the elastic behavior at low frequencies is reduced, exhibiting a lower plateau.

DSC results

The DSC results are summarized in terms of T_g and ΔC_p values in Table I. The material's T_g was not affected by the silica nanoparticles. As it is reported in the literature,[28] a wide variety of polymer nanocomposites have shown interesting changes in the
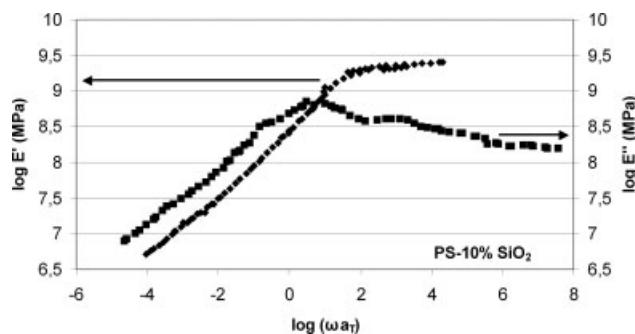

Figure 7 Master curves of storage modulus E' and loss modulus E'' of PS-10% SiO_2 in a reduced frequency scale, at a reference temperature of 95°C.

Figure 6 Master curves of storage modulus E' and loss modulus E'' of PS-8% SiO_2 in a reduced frequency scale, at a reference temperature of 95°C.

TABLE I
DSC Results

Sample type	T_g (°C)	ΔC_p (cal/g °C)
PS	90.31	0.282
PS-4%	90.92	0.294
PS-8%	90.92	0.276
PS-10%	90.70	0.275
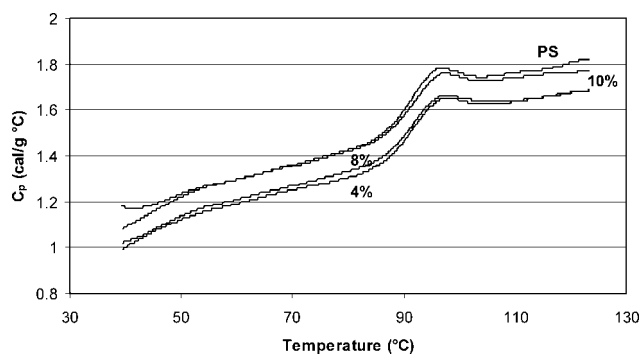
Figure 8 Specific heat capacity versus temperature, at a heating rate of 5°C/min for all materials tested.

Figure 9 Tensile true stress–strain curves with a strain rate of $2.77 \times 10^{-4} \text{s}^{-1}$, at 20°C, for all materials tested.

bulk glass transition behavior. Most researchers report an increase in the T_g as a function of filler content,[29–31] however, decreases in the T_g have also been found.[32–33] Especially for PS it has recently been found[34] that the T_g of PS is not impacted with the addition of silica nanofiller.

On the other hand, the specific heat capacity C_p is a fundamental physical property of a polymer and is related to the molecular structure and the polymer morphology. In Figure 8, typical DSC scans are plotted for all materials tested. In all cases an inflection zone in the C_p curve is observed. This inflection is an indication of the transition from the glass-like to the rubber-like state.

Moreover, the change of C_p, ΔC_p, at the glass transition temperature, is strongly connected with the polymer structure and describes the different values of thermal energy for the glass and rubber states, which are required for keeping the heating rate of the sample constant. The thermal energy absorbed by the sample increases the macromolecular mobility. When the amplitudes of the elementary vibrations reach a maximum, which corresponds to a resonance effect, the glass transition is approached and C_p takes a maximum value. After passing the transition region, the resonance effect disappears and C_p retains a rather constant value. From Table I and Figure 8, where the ΔC_p values are plotted in respect to temperature, it is shown that ΔC_p exhibits a maximum in the case of PS-4% and hereafter starts increasing. This nonmonotonic behavior of ΔC_p is another indication of the different type of silica dispersion into the PS matrix, compared to the other composites examined.

Tensile stress–strain results

Tensile experiments were performed at 20°C, at 85°C, which is a temperature close to T_g and at 100°C just above it. It was not possible to examine a higher than 100°C temperature, because of the flow behavior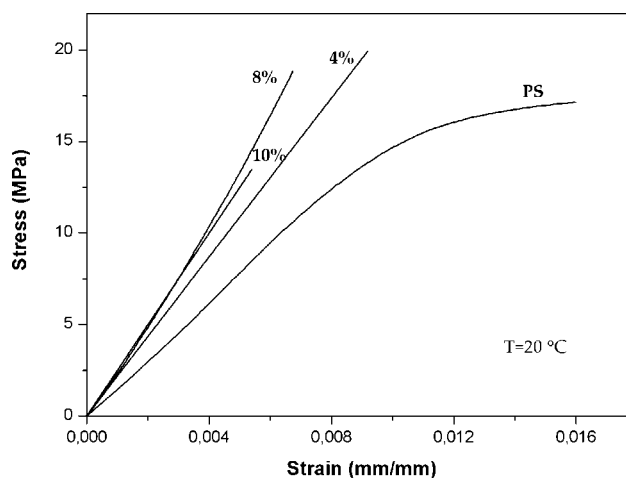 exhibited by the material. A quite different response is obtained at various temperatures. From Figure 9 it is shown that when the response is measured in the glassy region, a brittle behavior is observed for both pure PS and PS/SiO$_2$ nanocomposites. The elastic properties of the materials at all temperatures tested are presented in Table II. All types of nanocomposites show a higher tensile strength and a lower elongation at break, compared to pure PS that breaks at a strain of 0.016. The presence of silica results to an impressive increment of the Young modulus as is shown also in Table II.

It has been shown in Ref. 35 from molecular dynamics studies that the mobility of nanoparticles into the polymer can be decisive for introducing new energy-dissipating mechanisms that lead to enhanced toughness of the nanocomposite, while the mobility of polymeric matrix is a requirement for this mechanism to be effective. In glassy state, due to the restricted molecular mobility, such a mecha-

TABLE II
Tensile Results

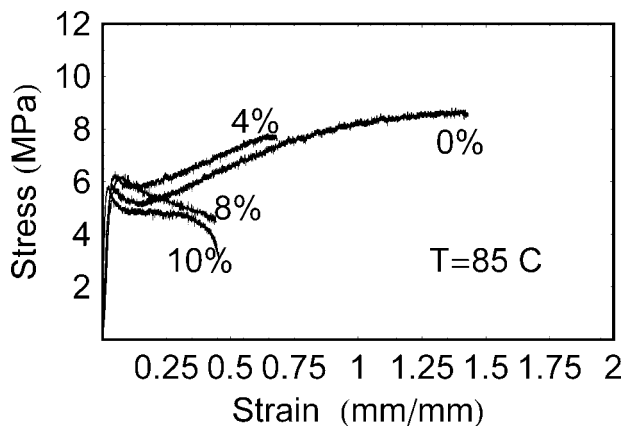| Sample type	Tensile modulus (MPa)	Yield (fracture) stress (MPa)	Strain at break
$T = 20°C$			
PS	1644.7	17	0.016
PS-4%	2257.3	20	0.0086
PS-8%	2739.7	19	0.0066
PS-10%	2500.0	13.5	0.0054
$T = 85°C$			
PS	288	5.9	1.47
PS-4%	360	6.4	0.7
PS-8%	650	6.2	0.43
PS-10%	450	5.8	0.48
$T = 100°C$			
PS	6.85	7.5	–
PS-4%	8.16	6.4	–
PS-8%	5.7	2.0	–
PS-10%	3.51	2.5	–

Figure 10 Engineering tensile stress–strain curves with a strain rate of 2.77×10^{-4} s^{-1}, at 85°C, for all materials tested.

nism cannot be activated. At 85°C, as it is depicted in Figure 10, the material response is completely different. Pure PS as well as PS/nanocomposites exhibit a sharp yield stress followed by a strain softening and a subsequent strain hardening in PS and PS-4%. Regarding yield stress and Young modulus a trend is revealed similar to that detected at 20°C, i.e., the nanoparticles enhance the mechanical response of the PS matrix. At high temperatures, close to the T_g, polymer chain, as well as particle mobility is increased, therefore polymer-particle interaction is enhanced. In this case, the interfacial region is enlarged and becomes more decisive to the macroscopic response. Especially in the case of 8% per weight, the modulus increment is more pronounced, and the elongation at break is higher, which is a strong indication that the aforementioned mechanism is accelerated in this case. This effect seems to be reversed for 10% per weight, where the mechanical properties of the nanocomposites start to deteriorate, probably due to particle agglomeration effects.

At 100°C as is presented in Figure 11, the materials appear to have a viscoplastic response, exhibiting a maximum yield stress followed by a smooth decrement up to high values of strain. The machine frame into the oven was not enough for the materials to attain their elongation at break. Regarding tensile properties, the same trend as at 85°C has been observed.

MODELING OF THE VISCOPLASTIC RESPONSE

In Figure 10, the main features of yielding, strain softening, and strain hardening are exhibited by the pure PS matrix, and the PS-4% nanocomposite. The PS-8% breaks after yielding and strain softening, showing no hardening. The same trend is observed for PS-10%. From all these results, it can be observed that strain softening is more intense for the nano-

composites, than for the pure matrix. The amount of strain softening is related to an evolution of structure, in other words to the evolution of free volume. The concept of free volume can be generalized to involve localized regions of holes, defects, and molecular segments that rearrange cooperatively for plastic flow to occur. The evolution of these regions with deformation has been used in a number of works[36–38] to simulate yielding and strain softening of polymers. Under the assumption that during deformation, strain is accumulated in those specific regions, which are randomly distributed into the deformed material, the total applied deformation will consequently be distributed inhomogeneously around these regions. When the distributed elastic energy around each region reaches a critical value, a nonreversible transition takes place, denoting the emergence of plastic deformation. If each one of these transitions proceeds with a certain rate, the macroscopic plastic deformation will occur with a rate proportional to the number of simultaneously appeared localized transformations.

The functional form of the rate of plastic deformation Γ_p, which is extracted under the assumption that strain accumulated around these regions, and was presented in a previous work,[25] follows a Gaussian distribution will thus be given by:

$$\Gamma_p = \frac{2\dot{a}}{s\sqrt{2\pi}} \int_0^a \exp\left[-\frac{1}{2}\left(\frac{a_i - \mu}{s}\right)^2\right] da_i \qquad (1)$$

where $\dot{a}$ is the imposed strain rate, μ of the distribution, s is the standard deviation, a is the stretch ratio.

To describe the yield and post yield behavior, a kinematic formulation that separates the elastic (viscoelastic) from plastic strain, developed by Rubin[39] and successfully applied in previous work,[24] will now be used. For a uniaxial deformation, the time evolution of the stretch ratio $\dot{a}_m$ of the viscoelastic
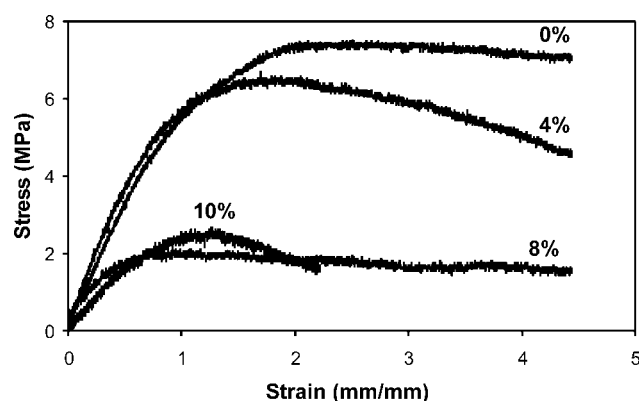

Figure 11 Engineering tensile stress–strain curves with a strain rate of 2.77×10^{-4} s^{-1}, at 100°C, for all materials tested.
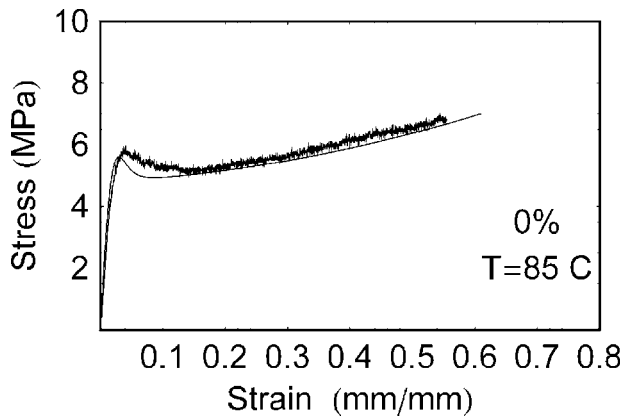
Figure 12 Tensile stress–strain curves with a strain rate of 2.77×10^{-4} s^{-1}, at 85°C, for pure PS. Thick lines: experimental data, thin lines: simulated results.
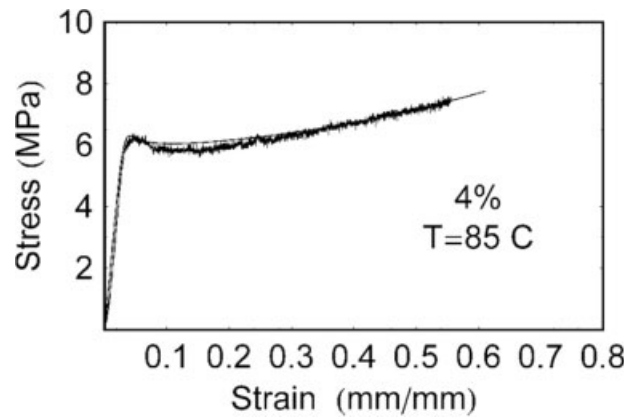

Figure 13 Tensile stress–strain curves with a strain rate of 2.77×10^{-4} s^{-1}, at 85°C, for PS-4% SiO$_2$. Thick lines: experimental data, thin lines: simulated results.

deformation is given in Ref. 39:

$$\frac{\dot{a}_m}{a_m} = f(a_m) \left[\frac{\dot{a}}{a} - \frac{\Gamma_p}{18} g(a_m) \right] \quad (2)$$

where $f(a_m)$, $g(a_m)$ are specific functions of the elastic stretch ratio a_m, $\dot{a}$ is the imposed strain rate, a is the stretch ratio and $a_m(0) = 1$. The mechanical response of the materials will be described with a constitutive equation, which is related to the aforementioned kinematic description by Rubin.[39] In the case of uniaxial tension, the stress will then be given by:

$$T_{11} = \mu J_m^{-1} \left(\frac{a_m^3 - 1}{a_m} \right) \quad (3)$$

where μ is the shear modulus, J_m is an equation of the form:

$$J_m = 1 + \frac{\mu}{3K} \left(\frac{a_m^3 - 1}{a_m} \right) \quad (4)$$

where a_m is the elastic stretch ratio, and K is the bulk modulus.

To further model the hardening response, the well known back stress tensor will be used, which defines the deformation resistance that the material has to overcome, due to the molecular alignment occurring after yielding and stress overshooting. This molecular alignment results in a change of the configurational entropy of the system.

Back stress, introduced in Ref. 40 is given by:

$$\mathbf{B} = C_R \frac{\sqrt{N}}{3} \left[\lambda_i L^{-1} \frac{\lambda_i}{\sqrt{N}} - \left(\frac{1}{3} \right) \sum_{j=1}^{3} \lambda_j L^{-1} \frac{\lambda_j}{\sqrt{N}} \right] \quad (5)$$

where λ_i is the plastic stretch ratio, λ_j is the stretch ratio in the other principal direction, which is

defined by the assumption of the isovolume deformation during yielding, C_R is the rubbery modulus and L^{-1} is the inverse Langevin approximation. N is the number of rigid chain links between physical molecular chain entanglements. The first component of tensor $\mathbf{B}$ is an additive term to the constitutive eq. (3).

Taking into account the set of eqs. (1)–(5) and making the integration of eq. (2) numerically, using small time steps with the software Mathematica,[41] the stress–strain response, depicted in Figure 10 could be simulated. The experimental results of Figure 10 were replotted within a lower scale of strain, so the initial response is more clearly presented. In Figures 12–14 the simulated stress-strain results in comparison with the experimental data are depicted.

The shear modulus μ, taken as the third of the tensile modulus, was estimated for the experimental stress strain results (Table II). Parameters C_R and N were fitted to be equal to 1.7 MPa and 12, respectively. For the case of PS-8%, C_R was taken equal to
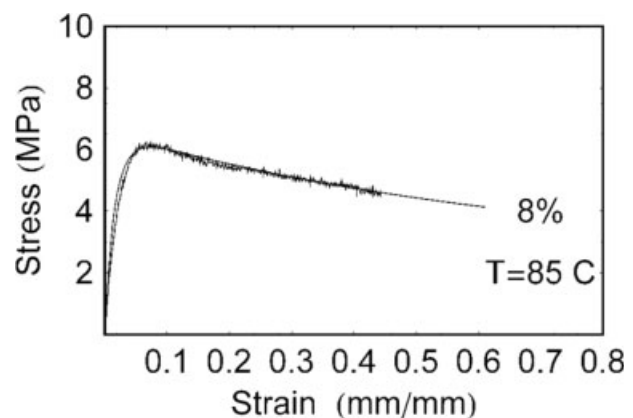
F12-F14

Figure 14 Tensile stress–strain curves with a strain rate of 2.77×10^{-4} s^{-1}, at 85 °C, for PS-8% SiO$_2$. Thick lines: experimental data, thin lines: simulated results.

zero, since no hardening response is exhibited by this material.

The parameters μ, s, related to the rate of plastic deformation and expressed by Eq. (1), determine the shape and the maximum value that the quantity Γ_p attains. Therefore, these parameter values render the details of the stress strain curve and mainly the strain softening effect. Parameter μ was equal to 0.005 for PS and equal to 0.0035 for the composites. Parameter s was equal to 0.018 for pure matrix, 0.0081 for PS-4% and 0.007 for PS-8%.

These parameter values, determining the shape and magnitude of the rate of plastic deformation, given by eq. (1), express the distributed nature of the material's structure. In the case of nanocomposites, due to the above assumptions, the aforementioned parameters attain a more specific physical meaning, expressing further the distribution of the interfacial region around dispersed particles. Therefore, it is extracted that for the pure PS matrix, a more wide structural distribution is evolved during deformation, and therefore a higher standard deviation, compared to that of the nanocomposites. Moreover, the maximum value of Γ_p for pure PS, which was calculated during the simulation procedure, was found to be lower than that of the composites, while the PS-4% sample appears to have the maximum value of the rate plastic deformation, for the best simulation. This is reversed for the PS-8% material. These observations can be related with the different size and extent of the localized regions that are developed, because of the presence of the silica particles. When the dispersed particles have a size in the nanoscale, the surface area of the dispersed phase becomes very large, resulting in an increase of the volume of interfacial region. Moreover, the radius of gyration of macromolecules and the interface width, become of the same order of magnitude. This effect results in some kind of homogenization and therefore in a more narrow distribution of localized regions, where strain is accumulated, and this is enhanced in the case of PS-4%.

CONCLUSIONS

The effect of SiO_2 nanoparticles on the thermomechanical properties of PS/SiO_2 nanocomposites, prepared with a melt mixing procedure was studied. Pure matrix and the corresponding nanocomposites with varying SiO_2 weight fraction up to 10% were extensively analyzed in terms of SEM, DSC, DMA, and tensile testing at three different temperatures. The optimum silica content was found to be about 4% per weight, and this can bring substantial improvement to the savings of the nanocomposites.

Silica contents above 8% were detrimental to the composite's macroscopic properties.

No T_g shifting was detected between the various material types, but the heat capacity change ΔC_p in the transition region, was found to increase with the silica content up to 4% per weight, while this trend is afterwards reversed. Apart from this, the relative position of the master curves of E' and E'' for the PS-nanocomposites, in a logarithmic frequency scale, provides a further evidence of the better particle dispersion in the case of PS-4% SiO_2.

The mechanical enhancement of the nanocomposites was manifested through the tensile stress–strain response, while the temperature effect was found to shift the response from a brittle one at 20°C, to a viscoplastic behavior at 85°C. This viscoplastic response has been modeled with a micromechanics model for the rate of plastic deformation, combined with a kinematic formulation developed elsewhere, that separates the elastic strain from the viscoplastic one. Model parameters, which have a molecular significance, were estimated and their dependence on silica content lead to results that are in accordance with those obtained by the experimental techniques applied.

References

1. Usuki, A.; Kojima, Y.; Kawasumi, M.; Okada, A.; Fukushima, Y.; Kurauchi, T.; Kamigato, O. J Mater Res 1993, 8, 1179.
2. Messersmith, P. B.; Giannelis, E. P. Chem Mater 1994, 6, 1719.
3. Sheng, N.; Boyce, M. C.; Parks, D. M.; Rutlege, G. C.; Abes, J. L.; Cohen, R. E. Polymer 2004, 45, 487.
4. Kojima, Y.; Usuki, A.; Kawasumi, M.; Okada, A.; Fukushima, Y.; Kurauchi, T.; Kamigato, O. J Mater Res 1993, 8, 1185.
5. Zhao, J.; Morgan, A. B.; Harris, J. D. Polymer 2005, 46, 8641.
6. Triantafillidis, C. S.; LeBaron, P. C.; Pinnavaia, T. J. J Solid State Chem 2002, 167, 354.
7. Ratna, D.; Manoj, N. R.; Varley, R.; Singh Raman, R. K.; Simon, G. P. Polym Int 2003, 52, 1403.
8. Wang, Z.; Pinnavia, T. J Chem Mater 1998, 10, 3769.
9. Burnside, S. D.; Giannelis, E. P. J Polym Sci Polym Phys 2000, 38, 1595.
10. Kontou, E.; Niaounakis, M. Polymer 2006, 47, 1267.
11. Lazzeri, A.; Zebarjad, S. M.; Pracella, M.; Cavalier, K.; Rosa, R. Polymer 2005, 46, 827.
12. Lee, K. M.; Han, C. D. Polymer 2003, 44, 4573.
13. Krishnamoorti, R.; Yurekli, K. Colloid Interface Sci 2001, 6, 464.
14. Wagener, R.; Reisinger, T. J. G. Polymer 2003, 44, 7513.
15. Ren, J.; Silva, A. S.; Krishnamoorti, R. Macromolecules 2000, 33, 3739.
16. Hoffmann, B.; Dietrich, C.; Thomann, R.; Friedrich, C.; Mulhaupt, R. Macromol Rapid Commun 2000, 21, 57.
17. Wang, J.; Pyrz, R. Compos Sci Technol 2004, 64, 925.
18. Brune, D. A.; Bicerano, J. Polymer 2002, 43, 369.
19. Lincoln, D. M.; Vaia, R. A.; Wang, Z. G.; Hsiao, B. S. Polymer 2001, 42, 1621.
20. Shelley, J. S.; Mather, P. T.; De Vries, K. L. Polymer 2001, 42, 5849.
21. Nam, P. H.; Maiti, P.; Okamoto, M.; Kotaka, T.; Hasegawa, N.; Usuki, A. Polymer 2001, 42, 9633.

22. van Es, M.; Xiqiao, F.; van Turnbout, J.; van der Giessen, E. In Specialty Polymer Additives; Al-Malaika, S.; Golovoy, A.; Wikie, C. A.; Eds. Blackwell Science: Malden, MA, 2001.
23. Yoon, P. J.; Fornes, T. D.; Paul, D. R. Polymer 2002, 43, 6727.
24. Spathis, G.; Kontou, E. J Appl Pol Sci 2001, 79, 2534.
25. Kontou, E.; Farasoglou, P. J Mater Sci 1998, 33, 147.
26. Wu, C. L.; Zhang, M. Q.; Rong, M. Z.; Friedrich, K. Compos Sci Technol 2002, 62, 1327.
27. Bartholome, C.; Beyou, E.; Bourgeat-Lami, E.; Cassagnaou, P.; Chaumont, P.; David, L.; Zydowicz, N. Polymer 2005, 46, 9965.
28. Ash, B. J.; Siegel, R. W.; Schadler, L. S. J Polym Sci Part B: Polym Phys 2004, 42, 4371.
29. Hergeth, W.; Steinau, U.; Bittrich, H.; Simon, G.; Schmutzler, K. Polymer 1989, 30, 254.
30. Iisaka, K.; Shibayama, K. J Appl Polym Sci 1978, 22, 3135.
31. Kotsilkova, R.; Fragiadakis, D.; Pissis, P. J Polym Sci Part B: Polym Phys 2005, 43, 522.
32. Arrighi, V.; Mc Ewen, I. J.; Qian, H.; Prieto, M. B. Polymer 2003, 44, 6259.
33. Sun, Y.; Zhang, Z.; Moon, K.-S.; Wong, C. P. J Polym Sci Part B: Polym Phys 2004, 42, 3849.
34. Rittigstein, P.; Priestley, R. D.; Torkelson, J. M. Annual Meeting and Fall Showcase Conference Proceedings 2005, Cincinnati, OH.
35. Shah, D.; Maiti, P.; Jiang, D. D.; Batt, C. A. Adv Mater 2005, 17, 525.
36. Hasan, O. A.; Boyce, M. C. Polym Sci Eng 1995, 35, 331.
37. Hasan, O. A.; Boyce, M. C.; Li, X. S.; Berko, S. J Polym Sci Part B: Polym Phys 1993, 31, 185.
38. Spathis, G.; Kontou, E. J Appl Pol Sci 1999, 71, 2007.
39. Rubin, M. B. Int J Solids Struc 1994, 31, 2615.
40. Wang, M. C.; Guth, E. J. J Chem Phys 1952, 20, 1144.
41. Wolfram, S. Mathematica, A System for Doing Mathematics by Computer, 4th ed.; Wolfram Research Inc: Champaign, IL, 1999.